communications earth & environment

Article

A Nature Portfolio journal

Article in Press

https://doi.org/10.1038/s43247-026-03969-z

Yellow River sediment sinks exhibit divergent decadal responses to anthropogenic and climatic forcing

Check for updates

Zhaoying Li[1] ✉, Naishuang Bi[2,3] ✉, Jeffrey A. Nittrouer[4], Kunpeng Sun[5], Yingjie Liu[6] & Houjie Wang[2,3]

Large river sediment sinks face profound reconfiguration under anthropogenic and climatic pressures. Using machine-learning-reconstructed daily suspended sediment concentration (SSC) records, we reveal a distinct divergence in decadal trends across the Yellow River sink system: proximal sinks show an ~18% mean decline in SSC, whereas distal sinks show a ~ 23% enrichment. This contrast emerges from two competing processes: anthropogenic sediment reduction and intensified winter-storm forcing that amplifies distal resuspension and lateral transport. Proximal depletion is driven by anthropogenic forcing, including an ~83% fluvial sediment reduction since the 1980s, a ~ 69% coastline solidification since the 1980s, and a ~ 30% seabed grain-size increase since the 1990s, which raise entrainment thresholds and inhibit resuspension. Conversely, distal sinks retain highly erodible sediments activated by more frequent winter storms and shortened inter-event durations. These findings highlight a critical Anthropocene regime shift: natural, fluvial-dominated source-to-sink continuums becoming systems governed by the asymmetric interplay of human engineering and climatic extremes.

The source-to-sink processes of riverine sediments, governing terrestrial-to-marine particulate transport from mountainous regions across the continental margins to the deep seafloor fans, constitute the fundamental drivers of erosion and deposition in land-ocean systems, playing a critical role in Earth's sedimentary cycle[1–3]. During the past half-century, the combined effects of climate change and human engineering activities, including increasing magnitude frequency of storm surges, dam construction, river discharge regulation, and sea-level rise, are fundamentally restructuring the mobilization, transport and sequestration of riverine sediment. These changes are most pronounced at terrestrial-marine interfaces, including deltas, estuaries, and coastal regions comprising near-shelf regions[4–6]. Systematic analysis of how variable human activities and marine environmental influences modulate shelf-to-sea and source-to-sink processes provides a significant and deeper understanding of nearshore material cycling and biochemical processes[7].

The Yellow River, as a typical anthropogenically stressed system, is regarded as a natural laboratory for contemporary sediment transport processes and represents a strategic microcosm of global deltaic systems (Fig. 1), as it possesses an extremely high sediment concentration that drives intense depositional activities from fluvial channels to the marine terminus in the Bohai Sea[8–11]. Previous studies on the sediment distribution pattern of the Yellow River in the marine environment have identified two distinct sink regions[12–14]. In this study, the proximal sinks are defined as the subaqueous deltaic clinoform of Laizhou Bay and Bohai Bay. The distal sinks are corresponded to the depocenters in the central Bohai Sea and along the coast of Shandong Peninsula (Fig. 1). Decadal-scale anthropogenic modifications, such as soil and water conservation projects and reservoir interception along the middle reaches, have caused decline in sediment delivery to the marine sink[15,16]. Furthermore, artificial flood pluses inducing episodic sediment delivery have resulted in rapid burial of terrestrial organic carbon and pollutants, fundamentally reshaping the spatio-temporal distribution of biogeochemical processes in the Bohai-Northern Yellow Sea[17–19].

Meanwhile, increasingly variable climatic conditions, particularly the increasing frequency of extreme weather events such as storm surges and hurricanes, have significantly influenced sedimentation in the sink region[20–22]. As a robust proxy reflecting the integrated sediment transport dynamic under varying environmental conditions, suspended sediment properties exhibit spatiotemporal heterogeneity in response to

[1]Ocean Science and Interdisciplinary Frontiers, Laoshan Laboratory, Qingdao, Shandong, China. [2]College of Marine Geosciences, Ocean University of China/Key Laboratory of Submarine Geosciences and Prospecting Technique, Ministry of Education, Qingdao, Shandong, China. [3]Laboratory for Marine Geology, Qingdao Marine Science and Technology Center, Qingdao, Shandong, China. [4]Department of Geosciences, Texas Tech University, Lubbock, TX, USA. [5]North China Sea Marine Forecasting Center of State Oceanic Administration, Qingdao, Shandong, China. [6]Oil & Gas Survey, China Geological Survey, Beijing, China.
✉e-mail: lzygeology@hotmail.com; binaishuang@ouc.edu.cn

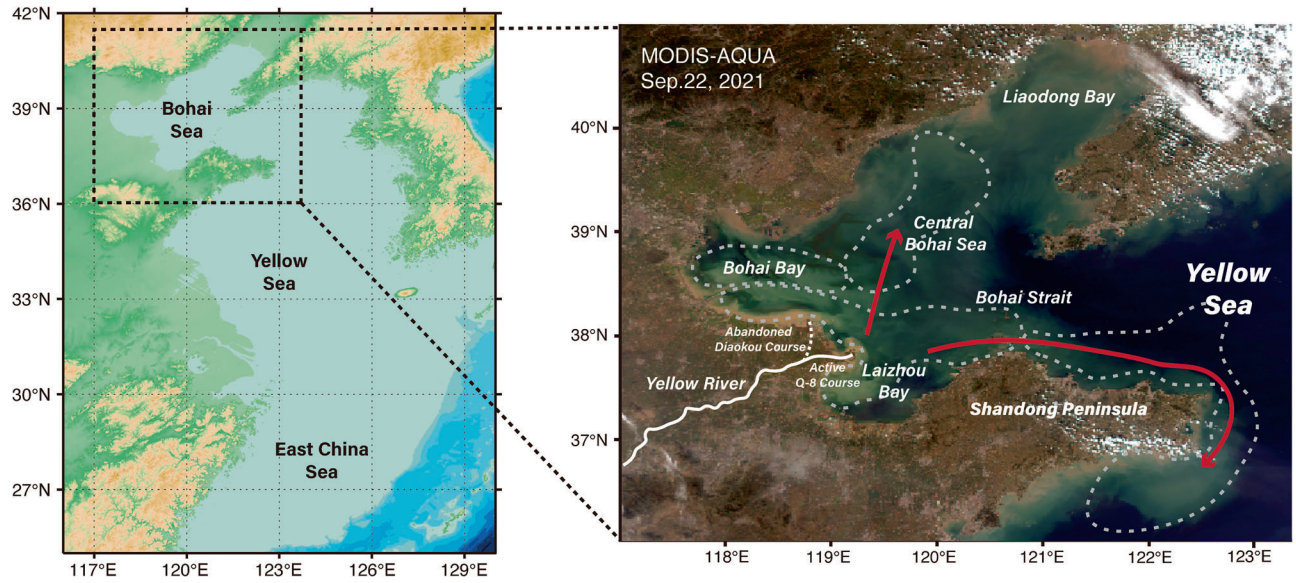


Fig. 1 | Study area and key sediment sinks of the Yellow River. The dashed area indicates the distribution of fine-grained fluvial source sediments. Red arrows indicate sediment transport pathways controlled by the winter monsoon[33]. The primary sediment sinks are located in Bohai Bay, Laizhou Bay, the Central Bohai Sea, and along the northern coast of the Shandong Peninsula. The map is modified from Qin, Mei[14], and Yang and Liu[13].

environmental forcings[23,24]. Previous studies have argued that intense winter monsoons accompanied by storm surges can generate powerful waves and significant sea-level oscillations, resuspending summer-deposited sediments for subsequent along-shelf distal transport via coastal currents[12,25,26]. Also, the reduction in riverine sediment supply and the coarsening of sediments in the subaqueous delta drives pronounced suspended sediment concentrations (SSC) depletion near the river mouth[27–29].

Therefore, it is imperative to execute a comprehensive quantitative analysis of variability trends in SSC within the sink area of the Yellow River, covering decadal time scales, so as to account for both anthropogenic and environmental changes. Nevertheless, the discontinuity in satellite data and the difficulty in acquiring in situ measurements render it challenging to quantify these changes. The majority of extant inter-decadal studies rely upon qualitative analyses of monthly mean data, which by nature tend to examine the entire study area in a holistic manner, and therefore lack accounting for spatial or temporal variation. Critical knowledge gaps persist regarding SSC dynamics in distal sinks, particularly within the depocenters off Shandong Peninsula's southern coastal zone and the central Bohai, where multi-decadal analyses remain conspicuously absent.

Machine learning (ML) techniques are valuable tools for optimizing the utility and continuity of satellite data[30]. In this paper, we apply the *SatelliteFixer* framework, an ML-driven gap-filling algorithm[31], to reconstruct daily SSC data from satellite data in the Bohai-North Yellow Sea system to examine the decadal variation in the sediment sinks areas of the Yellow River. Our analysis further resolves the compounding drivers that regulate the SSC fluctuations in proximal and distal sink regions. This paper investigates the decadal variability in the response of fluvial sediment sinks to climatic and anthropogenic forcing. We further aim to advance a mechanistic understanding of how increasingly intense anthropogenic and atmospheric processes are involved in the transfer of sediment across the river-shelf-ocean sink continuum. Specifically, this study addresses three objectives. First, to quantify decadal SSC trends across the proximal-distal sink continuum at daily resolution based on machine-learning-reconstructed satellite records. Second, to identify the dominant forcing controlling sediment dynamic in each sink zone. Third, to evaluate how anthropogenic and climatic factors reconfigure the river-shelf source-to-sink continuum under Anthropocene pressures.

Results

Decadal SSC distribution features

Based on the *SatelliteFixer* retrievals over an 18-year period (2002–2019), the annual mean SSC in the study area ranges from 0.81 mg/L to 38.95 mg/L (Fig. 3a), with the maximum and minimum values recorded in the Yellow River mouth and the central North Yellow Sea, respectively. Since sediment-laden gravity currents typically form via mixing with ambient seawater to govern cross-shelf sediment transport[32], the observable SSC serves as a reliable indicator of material deposition and transportation.

Maximum turbidity zones (peaking at 38.9 mg/L) are located in the southwestern Bohai Sea, encompassing Laizhou Bay and Bohai Bay, where both the active and abandoned deltas of the Yellow River are situated. As the primary sediment source, the Yellow River historically transports approximately 1.1 Gt/year of sediment to the ocean[8]. The majority is rapidly deposited near the river mouth, while a portion undergoes resuspension under hydrodynamic forces to form this SSC high-value area[12,24]. To categorize turbidity levels, a value of 9.7 mg/L (25% of the maximum annual mean value) was defined as the critical threshold separating high- and low-turbidity environments, and the relevant interval is delineated with dashed lines in Fig. 2. This turbidity boundary primarily reflects the dispersal pattern of fine-grained suspended sediment originating from the Yellow River plume, as well as those resuspended by hydrodynamic forcing such as tidal currents and waves. Furthermore, a tongue-shaped high-turbidity belt (10–15 mg/L) propagates along the northern shore of the Shandong Peninsula, consistent with the Shandong Coastal Current that forms an elongated mud deposit[13]. Another high-turbidity water mass protruding northeastward identifies a major sediment sink, reflecting seaward transport from the river mouth to the central Bohai Basin[33].

The regional SSC demonstrates pronounced seasonal variability characterized by "summer storage and winter transportation" (Fig. 2). During the winter half-year (October-March), intense northerly winds and associated waves facilitate the upward entrainment of terrigenous sediments to the surface layer[34], thus resulting in a high SSC regime across the entire Bohai Sea, especially near the Yellow River delta with the highest average SSC of ~125 mg/L. Additionally, high-turbidity water covering the proximal sinks (Laizhou Bay and Bohai Bay) spreads northward to the Bohai central basin and eastward to the Shandong Peninsula, forming the distal sink area[35]. Conversely, the summer half-year (April–September) features a calm hydrodynamic environment with a low regional mean SSC of ~2 mg/L.

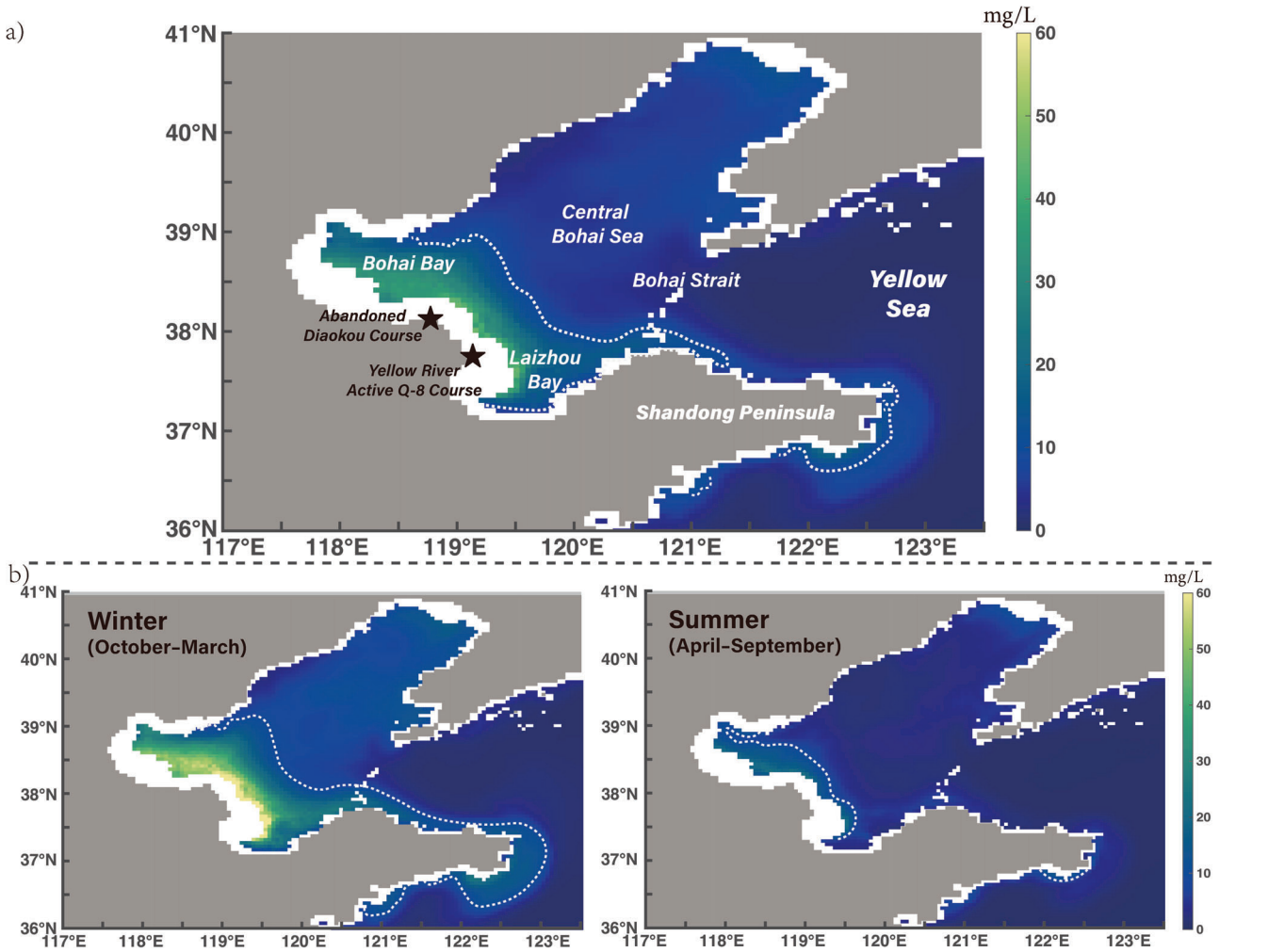


Fig. 2 | Spatial distribution of surface suspended sediment concentration (SSC) in the Bohai Sea and North Yellow Sea from 2002 to 2019. The high- and low-turbidity environments is separated marked by dashed lines. **a** Mean SSC. **b** Seasonal distributions during the winter and summer half-years.

During summer, the nearshore turbid belt indicates current-driven transport, while the distinct spatial contrast between the clear northern waters and the turbid southern waters of the Bohai Strait arises from the intrusion of the Yellow Sea Warm Current and tidal-current-induced resuspension, respectively[12,14].

Decadal variability of SSC

To evaluate the variation of SSC over the 18-year period, a Mann-Kendall trend analysis was conducted. The statistically significant results ($p < 0.05$, Fig. 3a, b) reveal contrasting spatial and temporal variations across the Bohai and Yellow Seas. A pronounced decline in SSC is observed in Bohai Bay, Laizhou Bay, and the western Liaodong Peninsula, with a maximum reduction approaching 80%. Conversely, the central Bohai Basin and the North Yellow Sea exhibit an elevated trend, particularly along the Shandong Peninsula, which demonstrates the highest increase of over 60%. The *SatelliteFixer* daily data provide an opportunity to examine the fluctuation of SSC over approximately 7000 days, and the typical cases illustrating the year-round trends are observed in Fig. 3c at Point A (37.8°N, 119.5°E) located in Laizhou Bay, Point B (39.0°N, 120.0°E) located in Bohai Central Basin, Point C (38.5°N, 118.9°E) located in Bohai Bay and Point D (36.5°N, 122.5°E) located near the Shandong Peninsula. Time-series extraction using the rLOESS method at four representative locations further validates this decadal divergence. Characterized by regular saddle-shaped seasonal oscillations, the SSC at these sites exhibits synchronized variability, indicating that the observed trends reflect a gradual shift rather than isolated extremes. The detrended results confirm that the proximal sinks (Points A and C) exhibit a declining trend, whereas the distal sinks (Points B and D) show an upward trend.

In this study, decadal variation is defined as significant when the change amplitude exceeds ±10%, with Fig. 4a depicting the geographical distribution of these areas. This threshold coincides with the 75th percentile of 18-year relative SSC change across MK-significant pixels, marking a natural break between ~75% with weak drifts <5% and ~25% with decadal-scale signals (10–80%) concentrated in the four sink zones. The identified areas demonstrate strong geographical correspondence with the sink area of the Yellow River, including the Bohai Bay proximal sink area (BBPS, with an 18-year mean value of 21.2 mg/L), the Laizhou Bay proximal sink area (LBPS, with an 18-year mean value of 13.4 mg/L), the central basin distal sink area (CBDS, with an 18-year mean value of 5.8 mg/L), and the Shandong Peninsula distal sink area (SPDS, with an 18-year mean value of 9.4 mg/L). The proximal sinks exhibit mean declines of approximately 18% (a net reduction of ~3.8 mg/L for BBPS and ~2.4 mg/L for LBPS), while the distal sinks increased by approximately 23% (a net increase of ~1.3 mg/L for CBDS and ~2.2 mg/L for SPDS).

To determine whether the observed annual-mean divergence between proximal and distal sinks is seasonally consistent or confined to a specific season, Fig. 4b decompose the Mann-Kendall trend results into winter-half-year (October-March) and summer-half-year (April–September)

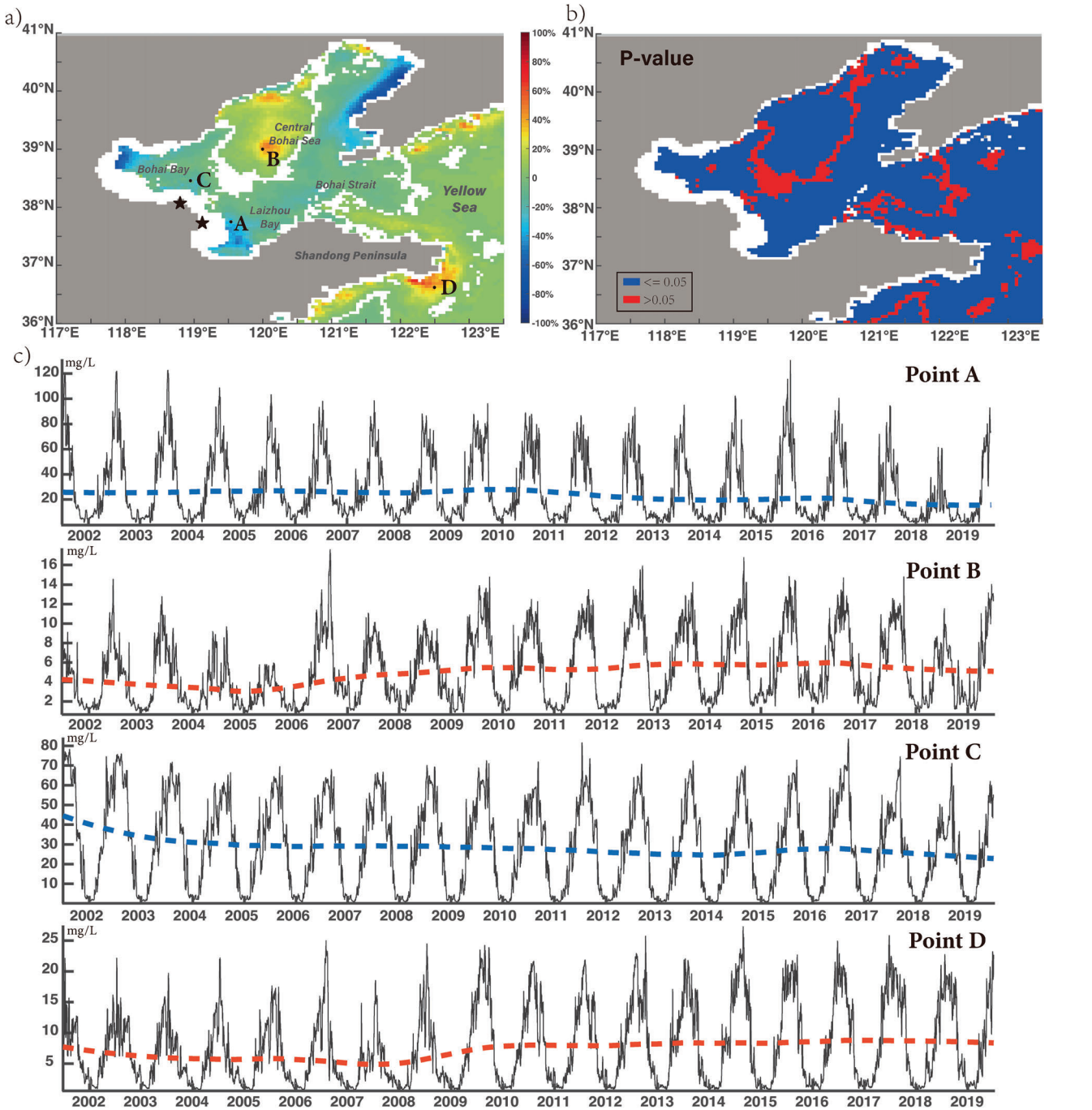


Fig. 3 | MK-test results of SSC in the Bohai Sea-North Yellow Sea. a Relative surface SSC change rate in Bohai Sea-North Yellow Sea derived from Mann-Kendall trend analysis, defined as the ratio of the total change over the 18-year period to the average-value in 2002. Points without 95% confidence level ($p \geq 0.05$) are excluded from the analysis. **b** Mann-Kendall p values, with red indicating non-significance ($p \geq 0.05$) and blue indicating significance ($p < 0.05$). **c** Daily SSC variation at Points A-D. Decadal trends (dotted lines) were extracted via rLOESS with 35% span (~ 2300 days, ~6 years), consistent with the trend directions identified by the Mann-Kendall analysis.

components. Specifically, the distal sinks exhibit a substantially stronger increasing trend during the winter half-year (exceeding 50% in parts of CBDS and SPDS) than during the summer, whereas the proximal sinks decline in both seasons. These results further reveal a seasonally consistent trend in spatial pattern, with a markedly higher magnitude of variability during the winter that is 1.1–2.3 times higher than that in the summer. During the summer, significant changes are primarily localized within five regions: the active river mouth of the LBPS (decreasing), the Diaokou abandoned delta (decreasing), the western BBPS (decreasing), the southern CBDS (increasing), and the coastal zone of the SPDS (increasing) (Table S1). The mean variation rate in these regions is approximately −22% in proximal sinks and 18% in distal sinks. During the winter months, the entire study area exhibits a pronounced variation in trend, with a marked increase in the distal sink (exceeding 50%) and a notable reduction in the proximal sink (~ 27%). Alterations exceeding 70% have been notably documented in four specific regions: the western portion of BBPS (decreasing), the southern region of LBPS (decreasing), the coastal zone of SPDS (increasing), and the majority of CBDS (increasing)(Table S1).

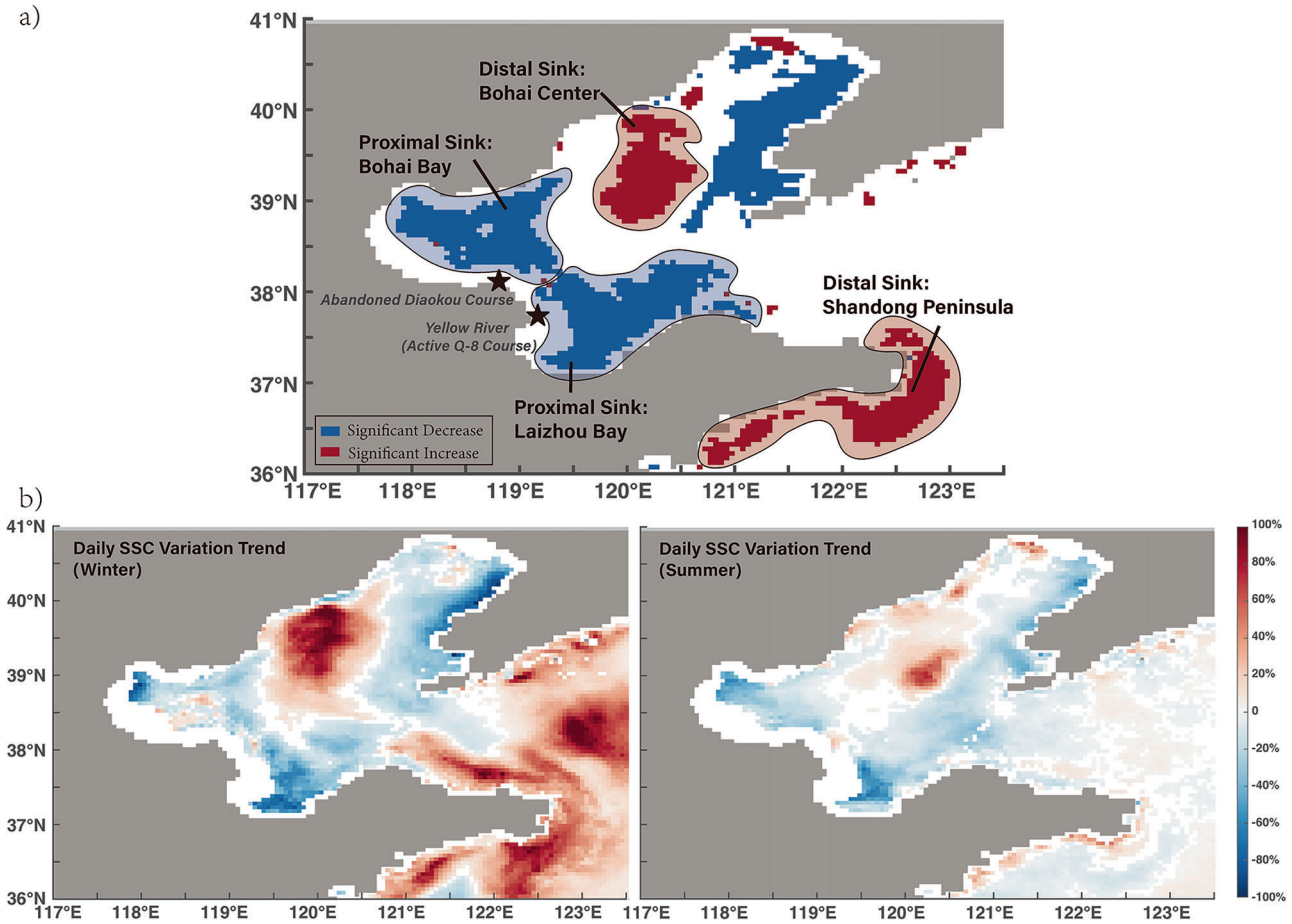


Fig. 4 | Variation trend of SSC in the Bohai Sea-North Yellow Sea. a Areas exhibiting significant decadal changes with red/blue denoting positive/negative anomalies. An area exhibiting a variation rate exceeding 10% of the 18-year mean value is deemed to exhibit significant variation. **b** The variation rate of the surface SSC in winter half year and summer half year by Mann-Kendall test, defined as the ratio of the half-year total change to the average-value in the initial half year (2002). Points without 95% confidence level ($p \geq 0.05$) are excluded from the analysis.

Temporal periodicities and forcing signals in yellow river sediment sinks

To quantify the long-term temporal variability of SSC across different sediment sinks, an evolutionary power spectrum analysis was applied to the daily SSC time series (2002–2019) at the four representative points and the results are shown in Fig. 5. The analysis focuses on frequencies below 0.035 cycles per day (cpd), corresponding to periods longer than ~1 month, to filter out sub-monthly variability. The results reveal that the annual signal dominates at all four points, while a secondary semi-annual signal is pronounced at the proximal sites and decays towards the distal sites, both surpassing the 95% confidence level of the robust autoregressive (AR) background. These correspond to an annual period (frequency ~0.00273 cpd, T ~ 366 days) and a semi-annual period (frequency ~0.00546 cpd, T ~ 183 days), where the period T is given by T = 1/f.

Data verify that the spectral power varies significantly across different regions. For the annual period, power intensities are highest and comparable at the proximal sink locations, recording ~144×10^3 at Point A and ~137×10^3 at Point C. In contrast, the annual power drops substantially in the distal sinks, decreasing to ~9×10^3 at Point D and reaching a minimum of ~3×10^3 in the central basin (Point B). A similar spatial pattern is observed for the semi-annual signal. Point A exhibits the highest semi-annual power of ~19×10^3, which accounts for about 13% of its corresponding annual peak. This absolute value decreases seaward to ~4×10^3 at Point C (representing 3% of its annual intensity), ~0.3×10^3 at Point D (2.9%), and is lowest at Point B with only ~0.05×10^3 (2%).

Discussion

Primary forcing mechanisms across diverse Yellow River sediment sinks

The SSC adjacent to Yellow River mouth exhibits high spatiotemporal variability, controlled synergistically by anthropogenic forcing and climatic drivers. Human interventions dominate the sediment source through regulating river water and sediment[36,37], while climate factors govern ocean dynamics by affecting sediment motion, transportation, and deposition[15,28]. As demonstrated by the temporal periodicities identified in Section 3.3, the entire study area is governed by a shared macro-forcing framework, specifically the annual monsoon cycle and riverine discharge patterns. Here, we first use the periodic signals to identify which forcing dominates each sink; the long-term changes in these two forcings are then examined in the following two sections.

To link these periodicities to their physical drivers, we compare the filtered SSC signal with the two candidate forcings: regional wind speed and fluvial sediment load (Fig. 6). The filtered data reveal that wind speed follows an annual oscillation, with peak intensities occurring during the winter monsoon. Conversely, the filtered Yellow River sediment load shows a distinct peak in summer. Using Point A as an example, its filtered SSC time series displays a "double-peak" pattern: one peak aligns with the winter wind maximum, and the other coincides with the summer fluvial sediment load. Notably, the two peaks are strongly asymmetric in amplitude, while the winter resuspension peak regularly exceeds 120 mg/L and the summer riverine peak reaches only ~20 mg/L. This mechanistic asymmetry between

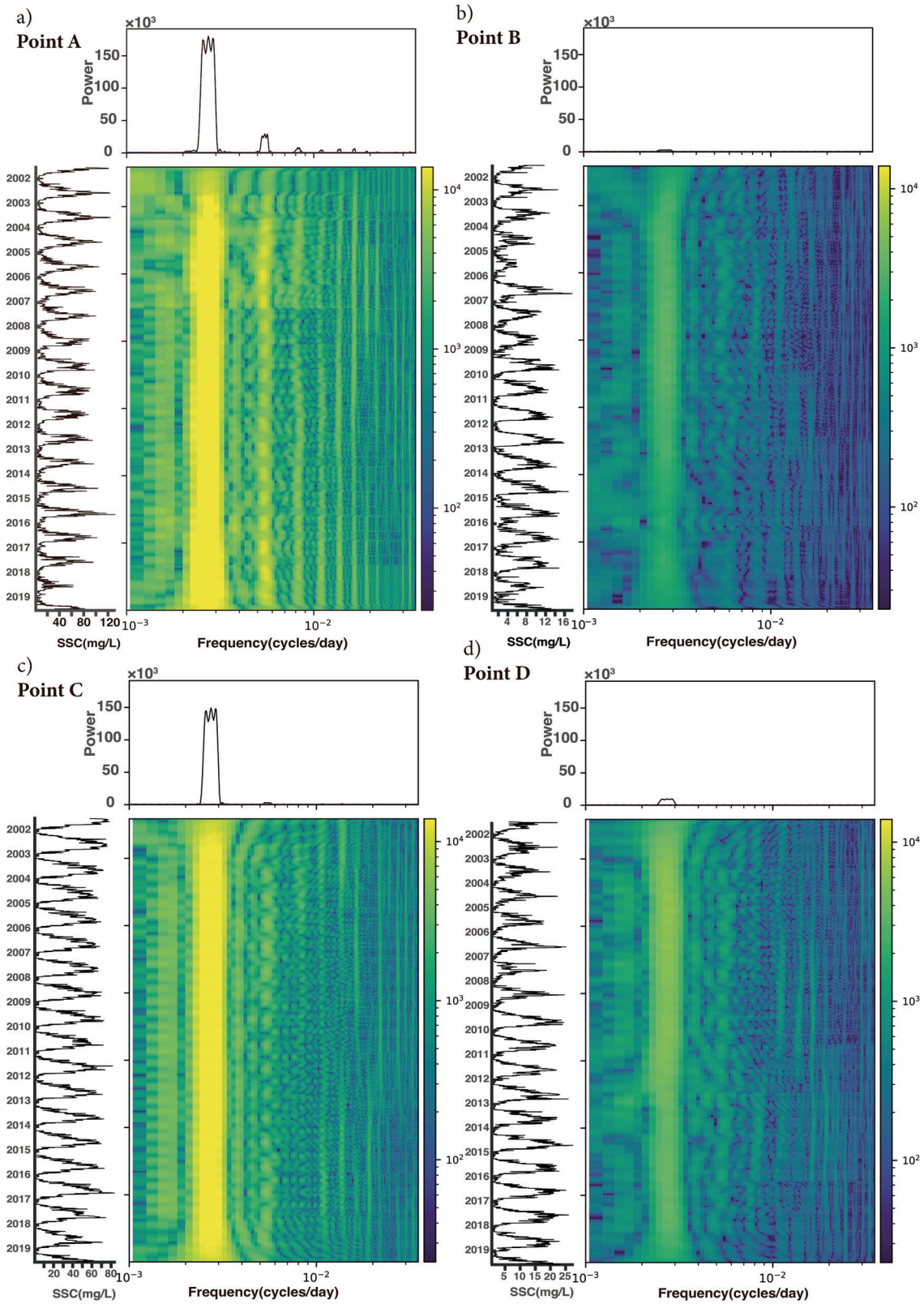


Fig. 5 | Evolutionary spectral analysis of daily surface SSC (2002–2019). a Result of Point A. **b** Result of Point B. **c** Result of Point C. **d** Result of Point D. Results integrate the original time series (left), the total power spectrum (top), and a central time-frequency spectrum where color intensity (deep red) denotes dominant periodicities.

the two seasonal maxima accounts for the co-existence of both annual and semi-annual spectral peaks in the power spectrum at Point A (Fig. 5a), with the amplitude of the semi-annual component (blue curve in Fig. 6a) directly quantifying the degree of contrast between two forcing-distinct seasonal peaks. Accordingly, the decrease of both filtered amplitudes towards 2018–2019 (Fig. 6a), despite the concurrent strengthening of the riverine signal (Fig. 6c), reflects a weakening of the winter resuspension peak that narrows the winter-summer contrast.

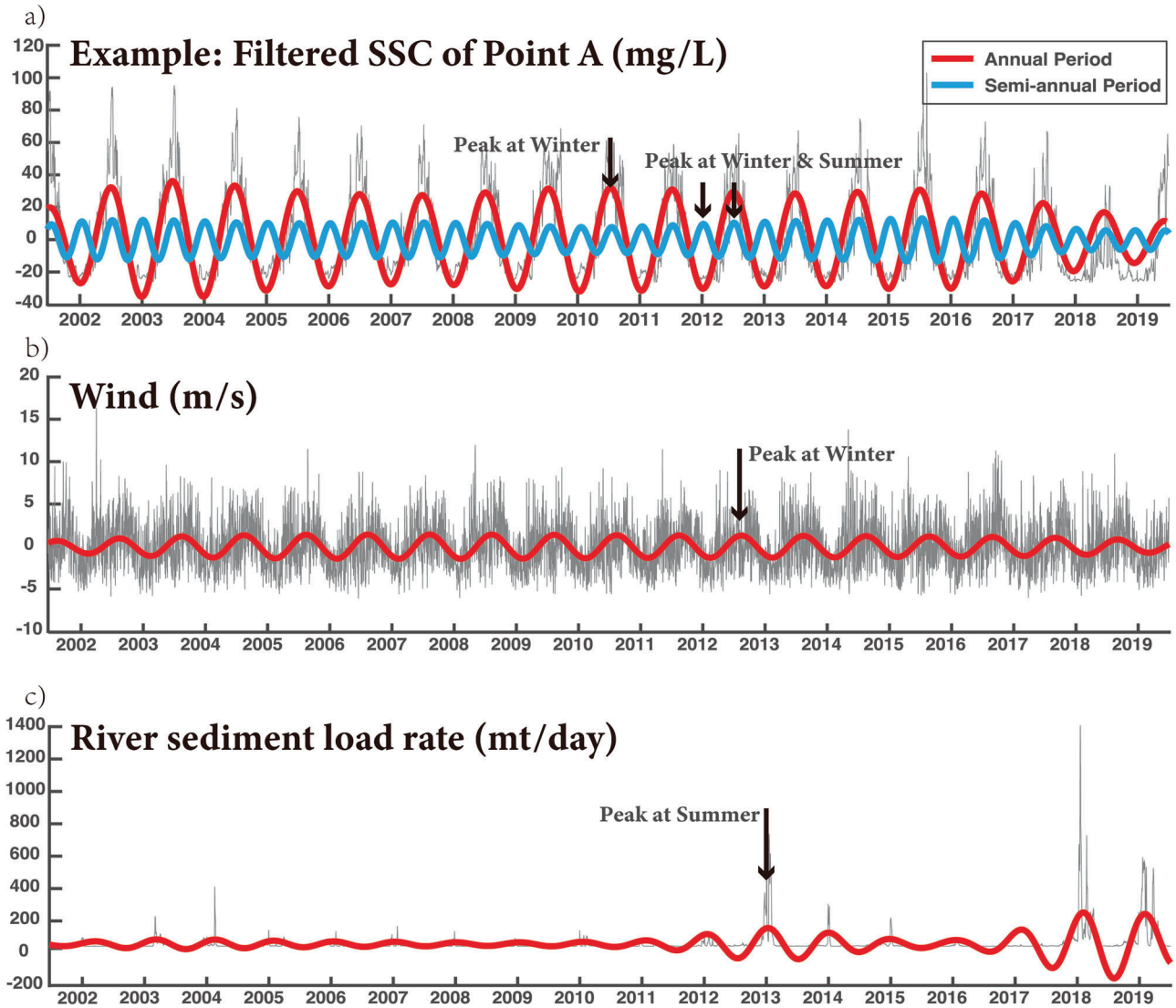


Fig. 6 | Time-series filtering results. a The representative results from Point A as an example. **b** The average wind speed in the study area. **c** The fluvial sediment load rate of the Yellow River. Note the synchronization of the filtered semi-annual peaks (blue) with the seasonal maxima of fluvial sediment load in summer and wind speed in winter.

In the proximal sinks (Points A and C), the dominant semi-annual periodicity is a product of the dual control. Wind-driven resuspension, which peaks during the intense winter monsoon, serves as the primary determinant of SSC variability and governs the annual cycle[38]. However, the massive delivery of riverine sediment near the active river mouth (Point A) during summer creates a secondary concentration peak that offsets the relative calm of the summer wind field. The interaction between these two opposing seasonal maxima effectively leads to the formation of the 183-day semi-annual periodicity. Consequently, the abundant sediment supply makes the proximal SSC highly sensitive to variations in wind speed. It should be noted that while Point C is also situated in the proximal sink area, its sediment is primarily derived from the erosion of the Diaokou subaqueous delta (abandoned in 1976) following its channel avulsion[39,40].

In contrast, the spatial decay of the riverine signal indicates that the far-field distal sinks are primarily forcing-dependent. The main difference governing SSC at Points B and D is their bathymetric characteristics. Situated in the central Bohai Basin, the water depth at Point B can reach 50–70 m. This increased depth acts as a physical shield that significantly attenuates the impact of wind-driven waves on the seabed, resulting in much weaker resuspension and, consequently, the lowest annual power among the four points. This bathymetric shielding explains why the central basin maintains relative low sediment concentration unless subjected to extreme hydrodynamic forcing.

Variations of human interventions in study area

Building on the forcing framework above, we first quantify the decadal changes in anthropogenic forcing. The Yellow River has historically been considered as the second-largest fluvial sediment source on Earth[41]. However, the artificial diversion of the primary channel from the Diaokou course to the present Qingshuigou course in 1981 initiated the profound influence of human activities on the regional spatiotemporal distribution of water and sediment[42]. Since the 1980s, the Yellow River has experienced an 83% decline in sediment flux (from 1.2 to 0.2 Gt/yr, Fig. 7a) owing to the cumulative impact of upstream dam construction, enhanced soil conservation efforts, and significant in-channel siltation[11,43]. This continuous declining trend was further exacerbated following the implementation of the Water and Sediment Regulation Scheme in 2002, which has had a considerable impact on the development of the deltaic lobe[39].

In addition to the reduction in riverine input, extensive human interventions have substantially restricted the availability of erodible sediments along the coast[44–46]. The construction of aquaculture ponds, shipping ports, and coastal dykes has led to a notable stabilization of the coastline. As

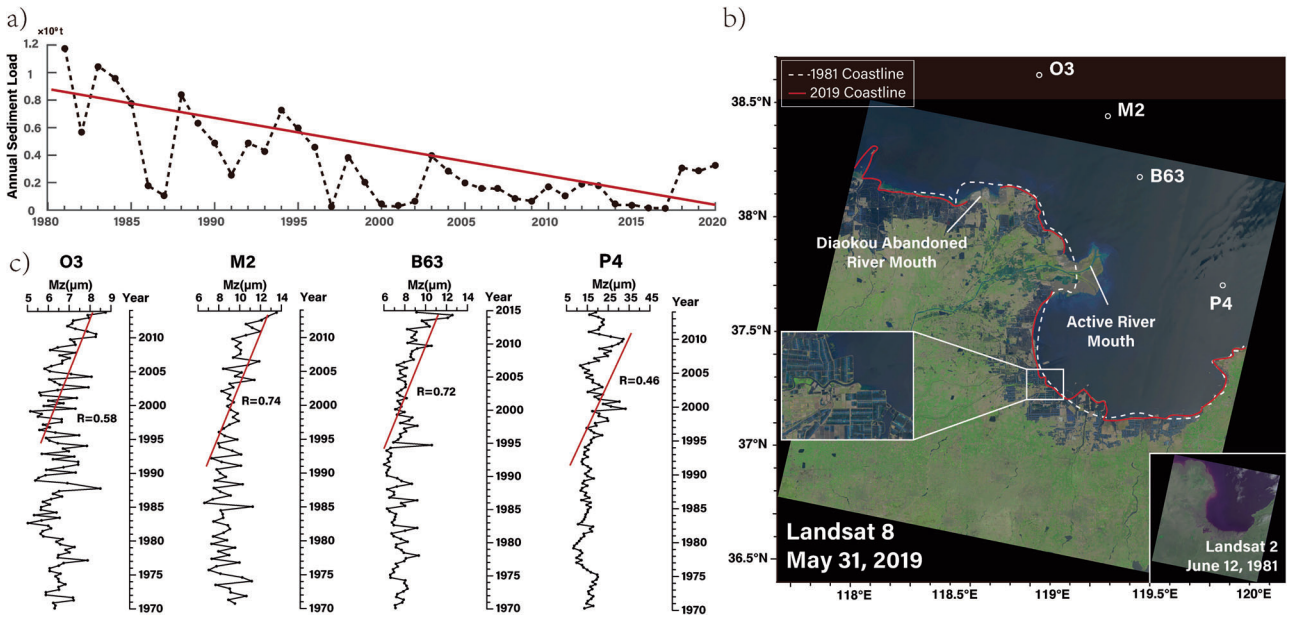


Fig. 7 | Variations of human interventions. a Sediment load and its decadal trend at Lijin Station from 1981, since the formation of the engineering-facilitated channelized river flow. **b** Comparative morphology of the Yellow River delta from Landsat imagery in 1981 (June 12, Landsat 2 Full-Resolution Natural Color image) and 2019 (May 31, Landsat 8 Full-Resolution Natural Color image). The dashed white line indicates the coastline in 1981. The red solid line indicates the artificial structures. **c** Temporal variation in mean grain size of sediments from Linear trends are fitted to the coarsening interval identified from the ^{210}Pb-dated record, spanning from the onset of systematic coarsening in the 1990s to the core top (~ 2015).

revealed by Lu, Zhang[46], reclamation was the predominant factor driving an approximate 72.9% seaward movement of the Bohai Sea coastline from 1985 to 2018. It is evident that as of 2018, approximately 69% of the original Bohai Sea coastline has been solidified by engineered modifications. Consequently, the contemporary morphology of the Yellow River mouth is markedly altered from its 1981 state, exhibiting near-complete artificial structures except for the active and abandoned river mouths (Fig. 7b).

This dual depletion of riverine and coastal sediment sources has fundamentally altered the physical properties of the regional sediment delivery and the deltaic substrate. The continuous scouring of coarse-grained sediment from the lower river reaches has resulted in sediment delivery characterized by intense coarsening and poor sorting[11,47,48]. Correspondingly, core samples collected in Laizhou Bay and Bohai Bay (Fig. 7c) demonstrate an average increase of more than 30% in mean grain size (*Mz*), indicating a gradual coarsening of the seabed. Crucially, this seabed coarsening off the delta coast significantly increases the critical shear stress required for sediment mobility. Based on the classical Shields threshold framework for non-cohesive equivalents (Soulsby, 1997), a 30% coarsening from a baseline fine silt of ~25μm theoretically yields an approximately 15.5% increase in the critical bed shear stress. However, in a natural estuarine system, the continuous winnowing of fine sediments creates a bed-armoring effect, which exponentially exacerbates the entrainment threshold beyond theoretical single-grain predictions. This physical effect acts as a powerful negative feedback mechanism, which undoubtedly inhibits sediment resuspension[27,29].

Variations of climatic drivers in study area

We next examine the changes in climatic forcing over the same period. Wind represents a pivotal driving mechanism for coastal sediment dynamics, primarily governing the resuspension of bed materials via wind-generated waves and modulating advective transport directions[33,49]. Regulated by the regular fluctuations of the East Asian Monsoon, the winter months predominantly dictate the annual sediment resuspension and transportation budget due to intense northerly winds and associated storm surges[12,25,38].

Under the context of global climate change, the study area has experienced a decadal intensification of extreme weather events. These storms can rapidly amplify wave-induced bottom stress, thereby enhancing sediment resuspension and dispersal across the benthic boundary layer[50–52]. Statistical analysis of winter storm events from 1981 to 2019, utilizing the method proposed by Fan, Chen[20], reveals a regional mean frequency of approximately 44.8 events per winter half-year and an average inter-event duration of 101.2 h (Fig. 8). During this period, the winter storm frequency increased significantly across the Bohai and North Yellow Seas. Specifically, regarding storm frequency and temporal intensity, the proximal sinks experienced a mean storm frequency increase of approximately 6.8%, accompanied by a 3.3% reduction in inter-event duration, indicating more concentrated and persistent storm impacts. Notably, this intensification of hydrodynamic forcing failed to yield elevated SSC in the proximal zones; rather, the enhanced storm-driven energy was counterbalanced by anthropogenic sediment depletion and the associated seabed coarsening discussed above.

Conversely, the distal sinks recorded a more modest mean storm frequency increase of approximately 2.5%, while the duration had no significant variation. However, isolated from direct coastal engineering and coursing sediment, the far-field distal seabed retains its fine-grained and highly erodible deposits, and this 2.5% amplification in winter storm frequency is sufficiently powerful to activate the benthic boundary layer. This enhanced wave-induced bottom stress efficiently fuels the resuspension-transport continuum. The winter-dominated amplification of the distal SSC increase (Fig. 4b) therefore confirms that this rise is primarily driven by intensified wave-induced resuspension rather than summertime riverine forcing.

The spatiotemporal asynchrony in sink areas

The differential evolution of the Yellow River sediment sink, as conceptualized in Fig. 9, is shown as a comprehensive system driven by the spatiotemporal asynchrony between high-intensity anthropogenic forces and climate change.

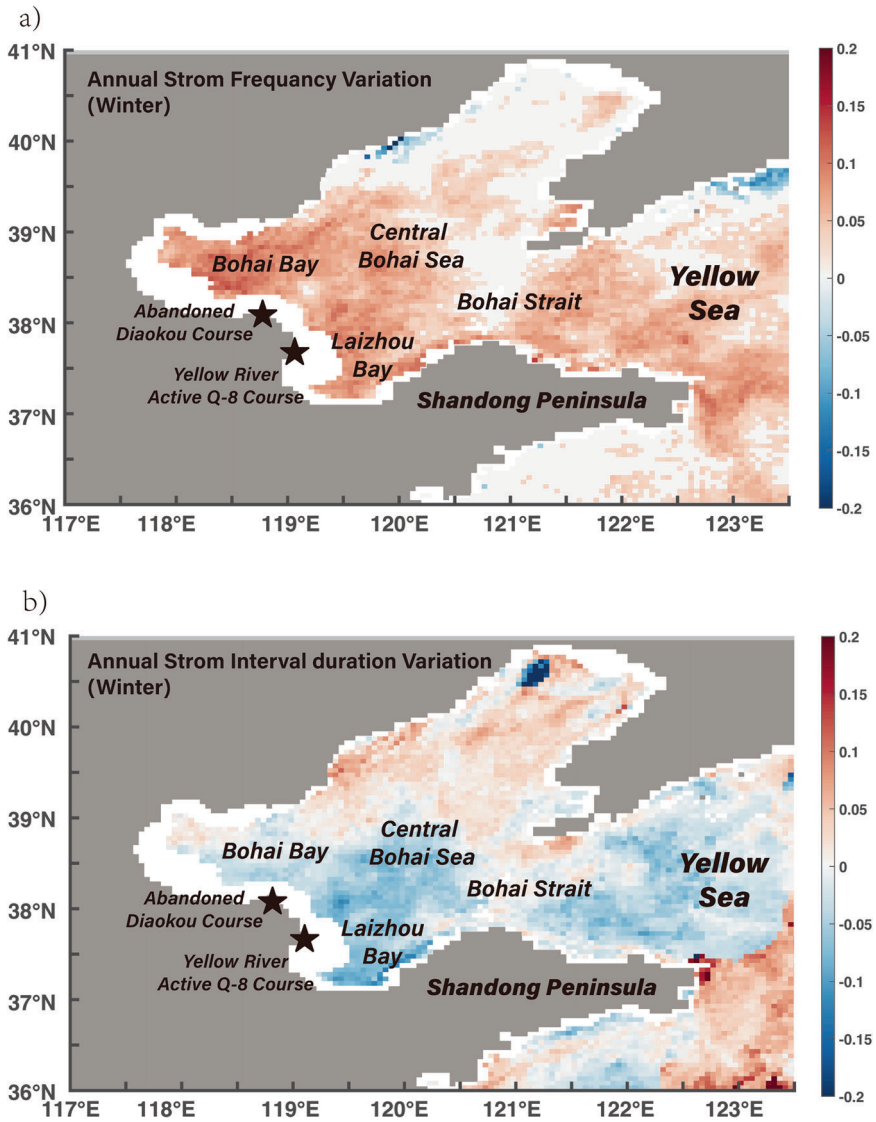


Fig. 8 | Variations of climatic drivers. a The variation rate of the annual storm frequency. **b** The variation rate of the annual storm interval duration in Bohai Sea-North Yellow Sea in winter season by Mann-Kendall test. The rates are defined as the ratio of the total change calculated by Theil-Sen slope value over the 38-year period to the average value in the initial year (1981).

In the proximal sinks, the sedimentary regime is overwhelmingly modified by human interventions across both the active and abandoned delta lobes. The fundamental driver for the decadal SSC declines across these nearshore regions is the dual shortage of sediment: a drastic reduction in Yellow River sediment flux combined with extensive shoreline reinforcing. This deprivation directly limits effective deltaic replenishment, leading to the progressive depletion of fine-grained materials and subsequent seabed coarsening. Consequently, the elevated entrainment threshold inhibits resuspension fluxes despite winter wind forcing[23]. However, the magnitude of this decline is different due to the proximity to the active river mouth, as the active channel still provides partial fine-grained replenishment to the LBPS[40]. In contrast, the BBPS completely lacks direct fluvial supply, relying only on the historical deposits of the abandoned Diaokou lobe. Without any effective modern replenishment, the seabed coarsening is even more pronounced at the BBPS, leading to a more severe and obvious reduction in SSC.

Unlike the proximal zones, decadal SSC variations in the distal sinks are predominantly controlled by climatic factors. Receiving Yellow River-sourced materials historically, the distal deposits consist primarily of fine sediments delivered via wind-driven transport under strong winter monsoons[53,54]. Lacking the direct impact of human activity, the surface sediments of far-field areas remain highly susceptible to wave-induced bottom stress. Specifically, across this river-delta-distal mud continuum, the suspended sediment in the distal sinks is sustained by a dual mechanism, including the local resuspension of the highly erodible fine-grained deposits driven directly by wave-induced bottom stress, and the lateral seaward transport of material delivered by intensified winter storms and the associated wind-driven coastal currents[33]. Both pathways are amplified by the decadal increase in winter storm forcing, driving the SSC enrichment observed in the distal surface waters.

A key point concerns the source of this lateral bottom transport, which is not contemporary fluvial input. Under the water-sediment regime of the Yellow River, the bulk of fluvial sediment is delivered during the summer flood season and rapidly deposited near the river mouth, whereas the large-scale seaward redistribution to the distal sinks occurs mainly in winter, when storms remobilize the pre-existing proximal inventory including the abandoned Diaokou subaqueous delta and the historical mud deposits of Bohai Bay and Laizhou Bay. This historical inventory is sufficient to sustain net seaward export even though modern fluvial supply has declined by ~83%, and the progressive seabed coarsening in proximal cores (Fig. 7c) provides direct geological corroboration of this net fine-sediment export. However, this regime likely represents a transient state. If the Yellow River continues to deliver such reduced sediment fluxes, the unreplenished delta and proximal sinks will struggle to sustain the present lateral export in the future, although the timescale of this transition remains to be constrained.

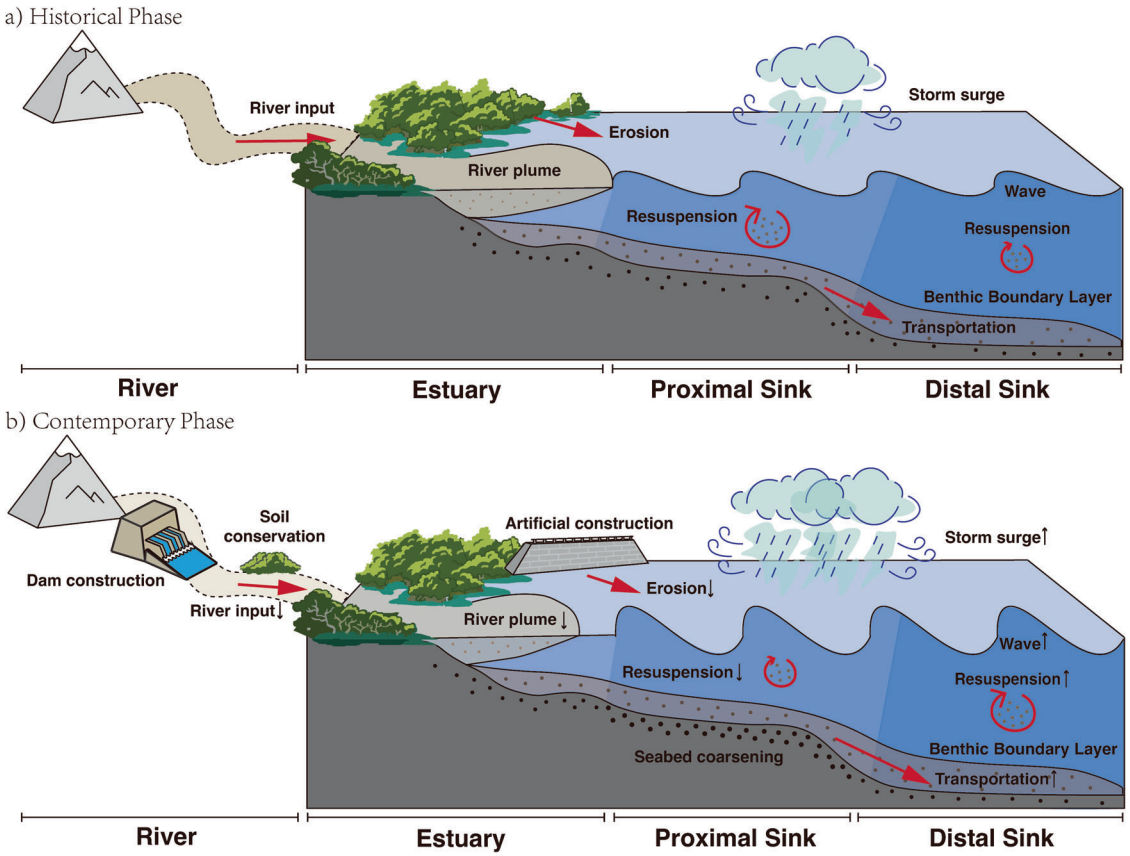


Fig. 9 | The spatiotemporal asynchrony in river sink areas. Conceptual diagrams contrasting the (**a**) historical phase and the (**b**) contemporary phase of the Yellow River source-to-sink system. The historical regime was dominated by fluvial sediment supply under moderate winter-monsoon forcing, whereas the contemporary regime is restructured by the coupling of human interventions and intensified winter storms, producing SSC depletion in proximal sinks and SSC enrichment in distal sinks. Arrow lengths schematically indicate the relative magnitude of sediment fluxes.

Broader implications for large river source-to-sink systems

Since the mid-20th century, the acceleration of anthropogenic activities and climatic extremes has fundamentally altered the sediment transportation in large river systems resulting in more irregular and complex processes[55,56]. Specifically, the opposite trend observed in the Yellow River sinks system are attribute to the regional evolutionary characteristics. However, more significantly, it reflects a broader global common feature shared by large river-shelf systems, which face analogous anthropogenic and climatic pressures[57]. Large river systems universally suffer from sediment reduction due to upstream dam impoundment, leading to deltaic erosion and a systemic decline in coastal turbidity. For example, the total sediment trapping capacity of reservoirs throughout the entire Yangtze River basin can reach ~450 million tons per year, resulting in a 60–70% reduction in sediment amount transported into the sea[58–60]. Concurrently, a distinct coarsening of subaqueous delta and Changjiang Distal Muds has been observed[61]. Similarly, the sediment load of the Mississippi River has been reduced by 50% through dam construction in the Mississippi Basin, resulting in the large-scale inundation of the river delta and wetlands[1], and the pristine sediment flux of Mekong River has declined from ~160 million tons per year to only ~25% of pre-1992 levels[62], while the trapping efficiency of all the planned reservoirs will be 51–69%[63]. Furthermore, extreme weather events have significant influence on sediment transport and morphological adjustments across these systems, while the increasing intensity and changing frequency of typhoons and hurricanes documented in the Northwest Pacific and the Gulf of Mexico provide the climatic forcing analog[22]. Similar to the Yellow River, the subaqueous delta of the Yangtze River and Mekong River experiences significant sediment resuspension under the influence of winter storm surges[64–66], whereas the Mississippi River delta is severely impacted by intense hurricanes[67].

Nevertheless, the Yellow River sink system exhibits distinctly more extreme sedimentary responses than these counterparts, owing to its unique hydrological and management characteristics. Characterized by exceptionally high sediment-to-water ratio, equivalent damming interventions produce a far more disproportionate reduction in fluvial sediment supply compared to the Yangtze or Mississippi systems[68]. Furthermore, in contrast to the anti-seasonal regulation mode of the Three Gorges Reservoir (TGR) on the Yangtze River, the episodic Water and Sediment Regulation Scheme (WSRS) delivers concentrated pulses of floodwater before the flood season that transport coarse-grained channel sands seaward in short period, which has rendered the Yellow River a fully human-controlled system that has effectively lost its natural hydrological regime[69]. This combination of extreme sediment-to-water ratio and fully engineered hydrological control places the Yellow River sink system at the leading edge of anthropogenic source-to-sink restructuring among the world's major river systems. Building on this analog perspective, the proximal-depletion and distal-enrichment asymmetry documented here provides a predictive template for anticipating how other heavily engineered river-shelf systems may reorganize as fluvial supply continues to decline and storm forcing continues to intensify. In this sense, the Yellow River functions as an early-stage observational analog for changes that may emerge more gradually in less impacted systems.

Beyond sediment dynamics, this divergent decadal regime carries direct consequences for organic carbon (OC) burial in marginal seas. The riverine organic carbon of the Yellow River was concentrated in the fine-grained fractions of the suspended sediments[70], which are the principal carriers stabilizing OC during cross-shelf transport[71], thus the same physical processes governing the SSC divergence documented above also reshape the fate of sedimentary OC. The loss of fine-grained substrates in the proximal

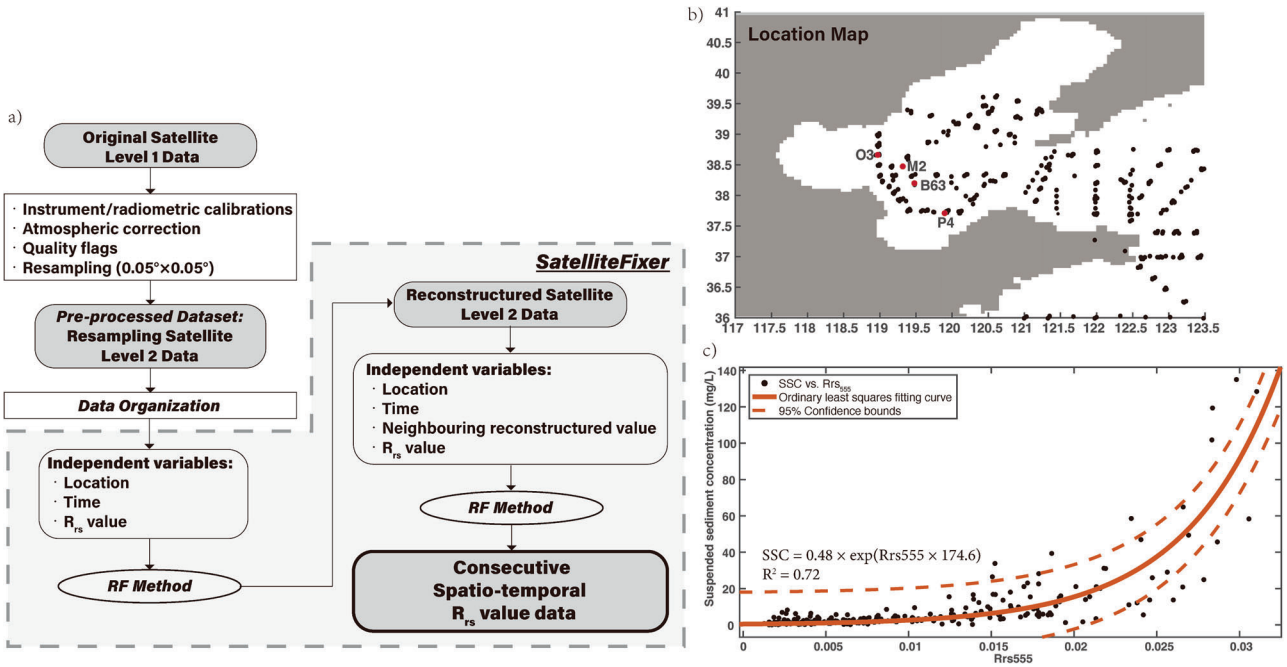


Fig. 10 | Methodology schematic and data validation. a Schematic flowchart of the satellite data reconstruction and improvement methodology (*SatelliteFixer*). **b** Map of cruise survey stations and sediment core locations. Data were collected during six cruises aboard the R/V *DONGFANGHONG 2* between April 2010 and July 2016, covering seasonal variations. **c** Fitting curve between in situ SSC and modeled $R_{rs}(555)$, with 95% confidence bounds. The exponential function is $SSC = 0.48 \times \exp(R_{rs} \times 174.6)$, with $R^2 = 0.72$.

sinks weakens mineral-bound OC stabilization, while the intensified storm-driven resuspension in the distal sinks repeatedly re-exposes previously buried OC to aerobic remineralization[2,72]. The cross-shelf reorganization of fine-sediment delivery thus likely drives a system-scale reduction in marginal-sea OC sequestration.

Our findings highlight a critical regime shift within the Anthropocene: the transition from a natural, fluvial-dominated system to one governed by the asymmetric interaction of human engineering and climatic forcing. The differential responses observed across the river-shelf-sea continuum reflect the complexity of Earth surface processes with anthropogenic activities, where the interaction of multiple Earth system spheres creates a new, spatiotemporally inconsistent sedimentary regime. Therefore, recognizing and characterizing the coupling of anthropogenic and climatic forcing becomes essential to understanding how the river-to-sea continuum will operate as a fundamental Earth-surface process under mounting Anthropocene pressures and climate change.

Methodology

Satellite observations and SSC retrieval

Daily surface SSC data in the Bohai and North Yellow Seas (36–41°N, 117–123.5°E) were derived using the *SatelliteFixer* model based on MODIS Aqua Level-1 data (July 2002-December 2019, 0.05°esolution). Prior to training, standard instrument calibrations and atmospheric corrections were applied to generate Level-2 products, with strict quality flags implemented to discard low-quality pixels of images impacted by conditions such as atmospheric correction failure, stray light, sun glint, radiance saturation, probable clouds, or ice contamination, etc. The original MODIS Aqua observations provide at most one overpass per day, and this quality screening leaves substantial data gaps: over the 18-year period (2002–2019, 6588 days in total), the number of valid retrievals per pixel ranges from ~300 to over 1,300, with a regional mean of approximately 800, and pixels with fewer than 300 valid observations were excluded from the analysis[31]. Valid-data density is lowest in the turbid nearshore and estuarine zones, consistent with the known limitations of ocean-color retrievals in optically complex coastal waters. The *SatelliteFixer* model utilizes a custom random forest architecture to reconstruct consecutive spatiotemporal data (Fig. 10a). The model takes four independent input features, including geographic location, time (encoded as continuous numerical variables of year and day-of-year), the raw R_{rs} value at the target pixel, and spatially neighboring reconstructed values from a first-pass prediction, which have no assumption of underlying periodicity or seasonal structure[31].

To validate the satellite-derived retrievals, continuous in situ SSC observations were conducted during six multidisciplinary cruises aboard the *R/V DONGFANGHONG 2* spanning different seasons: April 2010 (Spring, 6 days), May 2012 (Spring, 8 days), November 2014 (Autumn, 7 days), August 2015 (Summer, 8 days), January 2016 (Winter, 6 days), and July 2016 (Summer, 11 days). The locations of stations are shown in Fig. 10b. Equipped with Niskin bottles, CTD (SeaBird 911 plus) casts were deployed to collect water samples. 1000-mL water samples were filtered onboard using a GAST model pump through double-layer dry membranes for suspended sediment samples. After the cruises, filtered sediment samples were dried at 60 °C for 24 hrs and weighed with electronic balance (1/100,000 in resolution). SSC was calculated as the ratio of sediment mass to water volume.

Previous research has demonstrated a robust relationship between satellite data and SSC, typically modeled through exponential regression[12,73,74]. Fig. 10c demonstrates a robust exponential relationship with the modeled remote sensing reflectance at 555 nm (R_{rs555}), yielding an $R^2 = 0.72$. It should be noted that the R_{rs555} values used in this validation are drawn from the *SatelliteFixer*-reconstructed dataset, as the in situ cruises were conducted across all seasons including periods of low satellite data availability. The reconstruction accuracy of *SatelliteFixer* was independently assessed against ~70,000 withheld satellite observations never used in model training, yielding PCC = 0.98 for MODIS R_{rs555}, with quantile-quantile analysis confirming that the reconstructed data preserves the full statistical distribution of observed values[31]. This two-step validation, against independent in situ SSC measurements for the reconstructed product and against withheld satellite observations for the reconstruction itself, confirms

that the reconstructed dataset faithfully represents in situ sediment conditions across the full observed SSC range. Consequently, the quantitative inversion was performed using the following Eq.(1),

$$SSC = 0.48 \times \exp(R_{rs} \times 174.6) \quad (1)$$

while *SSC* represented suspended sediment concentration of sea surface (mg/L), and R_{rs} represented the MODIS Aqua R_{rs}555 data.

Boundary conditions and environmental forcing

Sediment cores, fluvial discharge records and meteorological data were collected to investigate the distribution trends and controlling factors of Yellow River-derived materials within the shelf sea. The sediment flux monitored at Lijin Station, which is the terminal hydrological station located approximately ~100 km upstream of the river mouth in the Bohai Sea, can be considered as the record of the Yellow River from 1980 to 2019. Four sediment cores were retrieved from prodelta regions of the Yellow River (Bohai Bay and Laizhou Bay) to measure the mean grain size (*Mz*), with core locations documented in Fig. 10b.

The ^{210}Pb-derived chronological framework places the core records on an absolute timescale from the 1970s to the collection year (~ 2015), with sedimentation rates of 0.43–0.72 cm/yr[27]. The exponential decrease of ^{210}Pb excess activity with depth (R^2 = 0.52–0.81) confirms stratigraphic continuity and minimal influence of vertical mixing. The grain size trend shown in Fig. 7c was fitted to the interval of systematic coarsening identified in the dated records (~ 1990s), corresponding to the documented reorganization of regional sediment supply following the 1976 channel diversion and the 1996 Qing-8 diversion, rather than to the full stratigraphic record which includes a pre-disturbance stable phase.

The winter storm surge, acting as an extreme weather event, is the key driver of sediment resuspension (via wind-waves) and transportation (via wind-driven currents). In this paper, a storm event is defined as a process with sustained wind velocities exceeding Beaufort Force 6 (10.8 m/s, 'Strong Breeze') for ≥6 h; meanwhile, the event separation criterion is specified as an interval of ≥24 h between two storm events. The frequency and gap duration were calculated based on wind data produced by the European Center for Medium-Range Weather Forecasts (ECMWF) dataset, which maintains four values reported daily, recording the *u* (eastward) component and *v* component at 0:00, 6:00, 12:00 and 18:00 hrs, during winter months (i.e., October to March). Given the shallow depth of the study area, storms exceeding Beaufort Force 6 generally induce full-water-column mixing; storm forcing was therefore characterized by event frequency and inter-event duration rather than by per-event intensity.

Statistical and time-series analyses

The Mann-Kendall test, a robust non-parametric statistical method for detecting monotonic trends in long-term time series[75,76] was utilized to quantitatively detect decadal trends in SSC variability across the study area (evaluated via the pyMannKendall package[77];).

Given an observation $X = x_1, x_2, \ldots, x_n$, the statistic S can be calculated using Eq. 2,

$$S = \sum_{i=1}^{n-1} \sum_{j=i+1}^{n} sgn(X_j - X_i) \quad (2)$$

where X_j and X_i are sequential data in the series and

$$sgn\left(X_j - X_i\right) = \begin{cases} 1\left(X_j - X_i\right) > 0 \\ 0\left(X_j - X_i\right) = 0 \\ -1\left(X_j - X_i\right) < 0 \end{cases} \quad (3)$$

As an indicator to measure the size of the trend, slope (β) calculated by Theil-Sen estimator can be expressed as Eq. 4

$$\beta = median\left(\frac{X_j - X_i}{j - i}\right) \forall 1 < i < j < n \quad (4)$$

when a positive value of β indicates an "uptrend" and a negative value of β indicates a "downtrend".

Served as complementary and independent corroboration of Mann-Kendall test, the robust locally estimated scatterplot smoothing (rLOESS) method was applied with a span of 35%[78], corresponding to a smoothing window of approximately 2300 days (~ 6 years) for the 6588-day time series. This window length is intentionally set to exceed the typical range of interannual climate variability (2–7 years) in the East Asian marginal seas, ensuring that the extracted trends reflect decadal-scale changes rather than interannual fluctuations. Furthermore, Evolutionary Spectral Analysis (ESA), a robust time-frequency analysis method for detecting shifts in dominant periodicities[79], was employed using the Acycle software[80] to trace the dynamic shifts of dominant periodicities (sliding window length equivalent to 35% of the data sequence, step size of 10). To isolate the periodic signatures of the various driving factors (e.g., wind speed and riverine load), Gaussian band-pass filtering was applied to the targeted frequency bands identified in the power spectrum[81].

Data availability

The satellite data used in this work were obtained from NASA's OceanColor Web (https://doi.org/10.5067/MODIS/MOD021KM.NRT.061). The wind data were obtained from the ECMWF ERA5 reanalysis, available through the Copernicus Climate Data Store (https://cds.climate.copernicus.eu/datasets/reanalysis-era5-single-levels). The river discharge data were provided by the Yellow River Conservancy Commission, Ministry of Water Resources of China (http://www.yrcc.gov.cn/gzfw/szygb). The gap-filled satellite suspended sediment concentration (SSC) data generated in this study, together with the Mann-Kendall test results and evolutionary spectral analysis results, is available at Zenodo (https://doi.org/10.5281/zenodo.21439725).

Code availability

The gap-filling algorithm used to process the satellite data is described in Li, Bi[31]. No custom code was developed for this study.

Received: 9 March 2026; Accepted: 14 August 2026;
Published online: 25 August 2026

References

1. Blum, M. D. & Roberts, H. H. Drowning of the Mississippi Delta due to insufficient sediment supply and global sea-level rise. *Nat. Geosci.* **2**, 488–491 (2009).
2. Leithold, E. L., Blair, N. E. & Wegmann, K. W. Source-to-sink sedimentary systems and global carbon burial: A river runs through it. *Earth-Sci. Rev.* **153**, 30–42 (2016).
3. Li, D. et al. Exceptional increases in fluvial sediment fluxes in a warmer and wetter High Mountain Asia. *Science* **374**, 599–603 (2021).
4. Syvitski, J. et al. Earth's sediment cycle during the Anthropocene. *Nat. Rev. Earth Environ.* (2022).
5. Wang, H. et al. Interannual and seasonal variation of the Huanghe (Yellow River) water discharge over the past 50 years: Connections to impacts from ENSO events and dams. *Glob. Planet. Change* **50**, 212–225 (2006).
6. Ganju, N. K. & Schoellhamer, D. H. Decadal-timescale estuarine geomorphic change under future scenarios of climate and sediment supply. *Estuaries Coasts* **33**, 15–29 (2010).
7. Hao, Z. et al. The changing Changjiang River estuarine-coastal ocean continuum in the anthropocene. *Catena* **238**, 107904 (2024).

8. Milliman, J. D. & Meade, R. H. World-wide delivery of river sediment to the oceans. *J. Geol.* **91**, 1–21 (1983).
9. Wang, H. et al. Stepwise decreases of the Huanghe (Yellow River) sediment load (1950–2005): Impacts of climate change and human activities. *Glob. Planet. Change* **57**, 331–354 (2007). p.
10. Mu, J. et al. Nutrient dynamics in the Yellow River-a case study of different reservoir regulation operations. *J. Hydrol.* **629**, 130563 (2024).
11. Wang, H. et al. Recent changes in sediment delivery by the Huanghe (Yellow River) to the sea: causes and environmental implications in its estuary. *J. Hydrol.* **391**, 302–313 (2010).
12. Bi, N. et al. Seasonal variation of suspended-sediment transport through the southern Bohai Strait. *Estuar., Coast. Shelf Sci.* **93**, 239–247 (2011).
13. Yang, Z. & Liu, J. A unique Yellow River-derived distal subaqueous delta in the Yellow Sea. *Mar. Geol.* **240**, 169–176 (2007).
14. Qin, Y.-C. et al. Sediment provenance and tidal current-driven recycling of Yellow River detritus in the Bohai Sea, China. *Mar. Geol.* **436**, 106473 (2021).
15. Zhou, Z. et al. Quantitative assessment on multiple timescale features and dynamics of sea surface suspended sediment concentration using remote sensing data. *J. Geophys. Res.: Oceans* **122**, 8739–8752 (2017).
16. Syvitski, J. P. et al. Impact of humans on the flux of terrestrial sediment to the global coastal ocean. *Science* **308**, 376–380 (2005).
17. Wang, H. et al. Impacts of the dam-orientated water-sediment regulation scheme on the lower reaches and delta of the Yellow River (Huanghe): A review. *Glob. Planet. Change* **157**, 93–113 (2017).
18. Wu, X. et al. Impact of artificial floods on the quantity and grain size of river-borne sediment: A case study of a dam regulation scheme in the yellow river catchment. *Water Resour. Res.* **57**, e2021WR029581 (2021).
19. Lu, T. et al. Transport of particulate organic carbon in the lower Yellow River (Huanghe) as modulated by dam operation. *Glob. Planet. Change* **217**, 103948 (2022).
20. Fan, Y. et al. Storm-induced hydrodynamic changes and seabed erosion in the littoral area of Yellow River Delta: A model-guided mechanism study. *Cont. Shelf Res.* **205**, 104171 (2020).
21. Zhu, Q. et al. Hidden delta degradation due to fluvial sediment decline and intensified marine storms. *Sci. Adv.* **10**, eadk1698 (2024).
22. Knutson, T. et al. Tropical cyclones and climate change assessment: Part II: Projected response to anthropogenic warming. *Bull. Am. Meteorol. Soc.* **101**, E303–E322 (2020).
23. Xie, B. et al. The spatio-temporal distribution and transport of suspended sediment in Laizhou Bay: Insights from hydrological and sedimentological investigations. *Front. Earth Sci.* **10**, 994258 (2022).
24. Li, P. et al. Spatiotemporal dynamics of suspended particulate matter in the Bohai Sea, China over the past decade from the space perspective. *Sci. Total Environ.* **851**, 158210 (2022).
25. Jin, S. et al. Drivers of suspended sediment dynamics along the shorelines of the Yellow River Delta detected from satellite data. *Earth Surf. Process. Landf.* **48**, 3091–3102 (2023).
26. Zhao, G. et al. Controlling factors and dynamic mechanisms of multidecadal changes of suspended sediment concentration in the Bohai Sea. *J. Geophys. Res. Oceans* **130** (2025).
27. Liu, L. et al. Coarsening of sediments from the Huanghe (Yellow River) delta-coast and its environmental implications. *Geomorphology* **401**, 108105 (2022).
28. Zhao, G. et al. Decadal variation and regulation mechanisms of the suspended sediment concentration in the Bohai Sea, China. *J. Geophys. Res.: Oceans* **127**, e2021JC017699 (2022).
29. Ji, H. et al. Spatiotemporal variability of suspended sediment concentration in the coastal waters of Yellow River Delta: Driving mechanism and geomorphic implications. *Mar. Geol.* **470**, 107266 (2024).
30. Goldstein, E. B., Coco, G. & Plant, N. G. A review of machine learning applications to coastal sediment transport and morphodynamics. *Earth-Sci. Rev.* **194**, 97–108 (2019).
31. Li, Z. et al. Improving blank ocean satellite data through machine learning: Case study and application in the Bohai Sea, China. *Marine Geol.* **107173** (2023).
32. Wright, L. et al. Effects of ambient currents and waves on gravity-driven sediment transport on continental shelves. *Mar. Geol.* **175**, 25–45 (2001).
33. Wang, A. et al. Sediment resuspension and transport due to synoptic winter winds in the Bohai Sea. *Geomorphology* **456**, 109211 (2024).
34. Qiao, L. et al. Seasonal transportation and deposition of the suspended sediments in the Bohai Sea and Yellow Sea and the related mechanisms. *Ocean Dyn.* **66**, 751–766 (2016).
35. Wang, A. et al. Seasonal variation in sediment transport and deposition on a muddy clinoform in the Yellow Sea. *Cont. Shelf Res.* **179**, 37–51 (2019).
36. Zhou, D. et al. Impacts of inland pollution input on coastal water quality of the Bohai Sea. *Sci. Total Environ.* **765**, 142691 (2021).
37. Ji, H. et al. Fluvial sediment source to sink transfer at the Yellow River Delta: Quantifications, causes, and environmental impacts. *J. Hydrol.* **608**, 127622 (2022).
38. Wang, H. et al. Seasonal distribution of suspended sediment in the Bohai Sea, China. *Cont. Shelf Res.* **90**, 17–32 (2014).
39. Bi, N. et al. Phase change in evolution of the modern Huanghe (Yellow River) Delta: Process, pattern, and mechanisms. *Mar. Geol.* **437**, 106516 (2021).
40. Wang, H. et al. Wave climate modeling on the abandoned Huanghe (Yellow River) delta lobe and related deltaic erosion. *J. Coast. Res.* **22**, 906–918 (2006).
41. Milliman, J. D. & Syvitski, J. P. Geomorphic/tectonic control of sediment discharge to the ocean: The importance of small mountainous rivers. *J. Geol.* **100**, 525–544 (1992).
42. Wu, X. et al. Stepwise morphological evolution of the active Yellow River (Huanghe) delta lobe (1976–2013): Dominant roles of riverine discharge and sediment grain size. *Geomorphology* **292**, 115–127 (2017).
43. Wu, Z. et al. Anthropogenic impacts on the decreasing sediment loads of nine major rivers in China, 1954–2015. *Sci. Total Environ.* **739**, 139653 (2020).
44. Bugnot, A. et al. Current and projected global extent of marine built structures. *Nat. Sustainabil.* **4**, 33–41 (2021).
45. Pianca, C., Holman, R. & Siegle, E. Shoreline variability from days to decades: Results of long-term video imaging. *J. Geophys. Res. Oceans* **120**, 2159–2178 (2015).
46. Lu, J. et al. The temporal evolution of coastlines in the Bohai Sea and its impact on hydrodynamics. *Remote Sens.* **14**, 5549 (2022).
47. Bi, N. et al. Impact of artificial water and sediment discharge regulation in the Huanghe (Yellow River) on the transport of particulate heavy metals to the sea. *Catena* **121**, 232–240 (2014).
48. Bi, N. et al. Response of channel scouring and deposition to the regulation of large reservoirs: A case study of the lower reaches of the Yellow River (Huanghe). *J. Hydrol.* **568**, 972–984 (2019).
49. Wright, L., Sherwood, C. & Sternberg, R. Field measurements of fairweather bottom boundary layer processes and sediment suspension on the Louisiana inner continental shelf. *Mar. Geol.* **140**, 329–345 (1997).
50. Kuang, C. et al. Sediment transport and morphological responses of a silty coast to a cold front event in the southwest Bohai Bay of China. *Estuar. Coast. Shelf Sci.* **278**, 108106 (2022).
51. Wang, C. et al. The impact of winter storms on sediment transport through a narrow strait, Bohai, China. *J. Geophys. Res.: Oceans* **125**, e2020JC016069 (2020).

52. Liu, X. et al. In-situ observation of storm-induced wave-supported fluid mud occurrence in the subaqueous yellow river delta. *J. Geophys. Res. Oceans* **127**, e2021JC018190 (2022).
53. Qiao, S. et al. Sediment accumulation and budget in the Bohai Sea, Yellow Sea and East China Sea. *Marine Geol.* S0025322717302955 (2017).
54. Lee, H. J., Jeon, C. K. & Lim, H. S. Dynamical analysis of the mud-belt formation in the Bohai, Yellow and East China seas. *Mar. Geol.* **423**, 106140 (2020).
55. Dethier, E. N., Renshaw, C. E. & Magilligan, F. J. Rapid changes to global river suspended sediment flux by humans. *Science* **376**, 1447–1452 (2022).
56. Zhang, T. et al. Shifted sediment-transport regimes by climate change and amplified hydrological variability in cryosphere-fed rivers. *Sci. Adv.* **9**, eadi5019 (2023).
57. Anthony, E. et al. Delta sustainability from the Holocene to the Anthropocene and envisioning the future. Nat. Sustainabil. **7**, 1235–1246 (2024).
58. Xu, K. & Milliman, J. D. Seasonal variations of sediment discharge from the Yangtze River before and after impoundment of the Three Gorges Dam. *Geomorphology* **104**, 276–283 (2009).
59. Dai, Z. et al. Decline in suspended sediment concentration delivered by the Changjiang (Yangtze) River into the East China Sea between 1956 and 2013. *Geomorphology* **268**, 123–132 (2016).
60. Gao, J. H. et al. Reservoir-induced changes to fluvial fluxes and their downstream impacts on sedimentary processes: The Changjiang (Yangtze) River, China. *Quat. Int.* **493**, 187–197 (2018).
61. Gao, J. H. et al. Rapid response of the Changjiang (Yangtze) River and East China Sea source-to-sink conveying system to human induced catchment perturbations. *Mar. Geol.* **414**, 1–17 (2019).
62. Van Binh, D., Kantoush, S. & Sumi, T. Changes to long-term discharge and sediment loads in the Vietnamese Mekong Delta caused by upstream dams. *Geomorphology* **353**, 107011 (2020).
63. Kummu, M. et al. Basin-wide sediment trapping efficiency of emerging reservoirs along the Mekong. *Geomorphology* **119**, 181–197 (2010).
64. Marchesiello, P. et al. Erosion of the coastal Mekong delta: Assessing natural against man induced processes. *Cont. Shelf Res.* **181**, 72–89 (2019).
65. Thanh, V. Q. et al. Modelling suspended sediment dynamics on the subaqueous delta of the Mekong River. *Cont. Shelf Res.* **147**, 213–230 (2017).
66. Chen, C.-T. A. et al. Enhanced buoyancy and hence upwelling of subsurface Kuroshio waters after a typhoon in the southern East China Sea. *J. Mar. Syst.* **42**, 65–79 (2003).
67. Blum, M. D. & Roberts, H. H. The Mississippi Delta Region: Past, present, and future. *Annu. Rev. Earth Planet. Sci.* **40**, 655–683 (2012). p.
68. Syvitski, J. P. M. et al. Sinking deltas due to human activities. *Nat. Geosci.* **2**, 681–686 (2009).
69. Wu, X. et al. Mega-reservoir regulation: A comparative study on downstream responses of the Yangtze and Yellow rivers. *Earth-Sci. Rev.* **104567** (2023).
70. Ge, T. et al. Sources and radiocarbon ages of organic carbon in different grain size fractions of Yellow River-transported particles and coastal sediments. *Chem. Geol.* **534**, 119452 (2020).
71. Blair, N. E. & Aller, R. C. The fate of terrestrial organic carbon in the marine environment. *Annu. Rev. Mar. Sci.* **4**, 401–423 (2012).
72. Bao, R. et al. Influence of hydrodynamic processes on the fate of sedimentary organic matter on continental margins. *Glob. Biogeochem. Cycles* **32**, 1420–1432 (2018).
73. Li, P. et al. Combining Landsat-8 and Sentinel-2 to investigate seasonal changes of suspended particulate matter off the abandoned distributary mouths of Yellow River Delta. *Mar. Geol.* **441**, 106622 (2021).
74. Doxaran, D. et al. Retrieval of the seawater reflectance for suspended solids monitoring in the East China Sea using MODIS, MERIS and GOCI satellite data. *Remote Sens. Environ.* **146**, 36–48 (2014).
75. Ali, R. et al. Long-term trends and seasonality detection of the observed flow in Yangtze River using Mann-Kendall and Sen's innovative trend method. *Water* **11**, 1855 (2019).
76. Kendall, M. G. The advanced theory of statistics. The advanced theory of statistics., 1946(2nd Ed).
77. Hussain, M. & Mahmud, I. pyMannKendall: a python package for non parametric Mann Kendall family of trend tests. *J. Open Source Softw.* **4**, 1556 (2019).
78. Cleveland, W. S. Robust locally weighted regression and smoothing scatterplots. *J. Am. Stat. Assoc.* **74**, 829–836 (1979).
79. Kodama, K. P. & Hinnov, L. A. Rock magnetic cyclostratigraphy (John Wiley & Sons, 2014).
80. Li, M., Hinnov, L. & Kump, L. Acycle: Time-series analysis software for paleoclimate research and education. *Comput. Geosci.* **127**, 12–22 (2019).
81. Weedon, G. P. Time-series analysis and cyclostratigraphy: examining stratigraphic records of environmental cycles. Cambridge University Press (2003).

Acknowledgements

We appreciate the editor and reviewers for their constructive comments that improved the quality of our manuscript.

Author contributions

Z.L. conceived the study and wrote the original draft. N.B. provided the data and supervised the project. J.A.N. reviewed and edited the manuscript. K.S. conducted the data collection. Y.L. performed the data analysis. H.W. supervised the project. All authors discussed the results and contributed to the final manuscript.

Funding

This research was primarily funded by the National Natural Science Foundation of China (NSFC, grants No. 42206172, 42476159 and 42330407), the Natural Science Foundation of Shandong Province (No. ZR2024QD004), and the Fundamental Research Funds for the Central Universities (Grants 202699002).

Competing interests

The authors declare no competing interests.

Additional information

Supplementary information The online version contains supplementary material available at https://doi.org/10.1038/s43247-026-03969-z.

Correspondence and requests for materials should be addressed to Zhaoying Li or Naishuang Bi.

Peer review information *Communications Earth & Environment* thanks Jianhua Gao, Jonah McLeod and the other, anonymous reviewers for their contribution to the peer review of this work. Primary Handling Editors: Somaparna Ghosh. A peer review file is available.

Reprints and permissions information is available at http://www.nature.com/reprints

Publisher's note Springer Nature remains neutral with regard to jurisdictional claims in published maps and institutional affiliations.

Open Access This article is licensed under a Creative Commons Attribution-NonCommercial-NoDerivatives 4.0 International License, which permits any non-commercial use, sharing, distribution and reproduction in any medium or format, as long as you give appropriate credit to the original author(s) and the source, provide a link to the Creative Commons licence, and indicate if you modified the licensed material. You do not have permission under this licence to share adapted material derived from this article or parts of it. The images or other third party material in this article are included in the article's Creative Commons licence, unless indicated otherwise in a credit line to the material. If material is not included in the article's Creative Commons licence and your intended use is not permitted by statutory regulation or exceeds the permitted use, you will need to obtain permission directly from the copyright holder. To view a copy of this licence, visit http://creativecommons.org/licenses/by-nc-nd/4.0/.

© The Author(s) 2026

This Article in Press is shared early to give you faster access to new research. It is citable and carries a permanent DOI. The final edited version will replace it automatically.